

ALEN: A Dual-Approach for Uniform and Non-Uniform Low-Light Image Enhancement

Ezequiel Perez-Zarate¹, Oscar Ramos-Soto², Diego Oliva², Marco Perez-Cisneros²

¹School of Computer Science and Technology, Zhejiang Gongshang University, , Hangzhou, 310018, Zhejiang, China.

²Departamento de Ingeniería Electro-fotónica, Universidad de Guadalajara, Av. Revolución 1500, Guadalajara, 44430, Jalisco, México.

Contributing authors: isaias.perez@alumnos.udg.mx; oscar.ramos9279@alumnos.udg.mx; diego.oliva@cucei.udg.mx; marco.perez@cucei.udg.mx;

Abstract

Low-light image enhancement is an important task in computer vision, essential for improving the visibility and quality of images captured in non-optimal lighting conditions. Inadequate illumination can lead to significant information loss and poor image quality, impacting various applications such as surveillance, photography, or even autonomous driving. In this regard, automated methods have been developed to automatically adjust illumination in the image for a better visual perception. Current enhancement techniques often use specific datasets to enhance low-light images, but still present challenges when adapting to diverse real-world conditions, where illumination degradation may be localized to specific regions. To address this challenge, the Adaptive Light Enhancement Network (ALEN) is introduced, whose main approach is the use of a classification mechanism to determine whether local or global illumination enhancement is required. Subsequently, estimator networks adjust illumination based on this classification and simultaneously enhance color fidelity. ALEN integrates the Light Classification Network (LCNet) for illuminance categorization, complemented by the Single-Channel Network (SCNet), and Multi-Channel Network (MCNet) for precise estimation of illumination and color, respectively. Extensive experiments on publicly available datasets for low-light conditions were carried out to underscore ALEN's robust generalization capabilities, demonstrating superior performance in both quantitative metrics and qualitative assessments when compared to recent state-of-the-art methods. The ALEN not only enhances image quality in terms of visual perception but also represents an advancement in high-level vision tasks, such as semantic segmentation, as presented in this work. The code of this method is available at <https://github.com/xingyumex/ALEN>.

Keywords: Low-light image enhancement, Low-level vision, Deep learning, Visual perception improvement

1 Introduction

Images taken under low-light conditions, such as indoors and or dark outdoor environments, both day and night, present a significant challenge in the correct visual perception due to the limited

light reflected by objects. The reduced image quality with color distortions and noticeable noise impacts fields like transportation surveillance [1], professional photography [2], and even in the recent implementation of autonomous driving [3].

These image conditions not only affect visual perception but also the performance of high-level vision tasks, such as object detection [4–7] and semantic segmentation [8–10].

To overcome this issue, several image enhancement strategies have been developed. Traditional techniques, such as histogram equalization [11–16], have been widely used to adjust contrast and improve image visibility. However, these methods are often insufficient as they fail to adequately capture local lighting variations and enhance both textural and chromatic details. On the other hand, the Retinex theory [17], divided into its respective categories: Single-scale Retinex (SSR) [18], Multi-scale Retinex (MSR) [19], and Multiscale Retinex with Color Restoration (MSRCR) [20, 21], proposes that a low-light image can be decomposed into a reflectance component and an illumination component. By manipulating these components, a better illumination-corrected image can be obtained. Despite significant advancements in these methods, they present limitations when applied directly in the RGB space due to challenges in concurrently learning brightness features.

In recent years, approaches based on convolutional neural networks (CNNs) [22], generative adversarial networks (GANs) [23], and transformers [24, 25] have shown significant progress in enhancing low-light images. Despite its advancements and achieving the best results in the visual enhancement of low-light images, these methods still face challenges in generalization across different datasets, which can lead to a tendency to amplify noise and produce unnatural or oversaturated colors in real-world image datasets [26–29].

To overcome these limitations and inspired by the Low-Light image enhancement algorithm (LoLi-IEA) [30], a novel method called the Adaptive Light Enhancement Network (ALEN) is introduced, addressing both local/global luminance adjustment and color restoration. This strategy is divided into three sections. The first step classifies whether image enhancement will be local or global based on the RGB color space, and the second step estimates the illumination accordingly, based on the previous classification. Finally, the last section ensures the attainment of more realistic and vivid colors. This approach aims to provide a robust and efficient solution for enhancing images under

low-light conditions, whether uniform or non-uniform illumination deficiencies. Several evaluations, including quantitative and qualitative assessments, were implemented to compare this proposal against state-of-the-art methods, confirming the efficiency of this proposal. Also, a high-level vision task, specifically segmentation, is conducted in processed images through this method, proving its efficiency in this task.

In summary, this proposal makes the following key contributions:

- **A novel approach to enhance both uniform and non-uniform image light conditions:** The ALEN technique is introduced, which is constructed from three distinct sub-networks: Light Classification Network (LCNet) for illumination classification, Single-Channel Network (SCNet) for single channel estimation, and Multi-Channel Network (MCNet) for multi channel estimation.
- **A new dataset for illuminance classification:** The Global-Local Illuminance (GLI) dataset is introduced, which is based on human perception and histogram analysis to categorize illuminance enhancement as either global or local.
- **A novel dataset for evaluating real-world low-light images:** The Diverse Illumination Scene (DIS) dataset is presented, encompassing real-world low-light images in various indoor and outdoor scenes, spanning both day-time and night-time periods.
- **A preprocessing tool for semantic segmentation enhancement in low-light images:** This proposal represents an improvement in semantic segmentation results when images with inadequate illumination are processed, leading to more accurate and reliable segmentation outcomes.

The remainder of the paper is structured as follows: Section 2 presents the most relevant related work, while Section 3 introduces the proposed method. Section 4 details the experiments and results obtained, and finally, Section 5 presents the conclusions and future work.

2 Related Work

Over the past decades, the enhancement of low-light images has been explored through a variety of

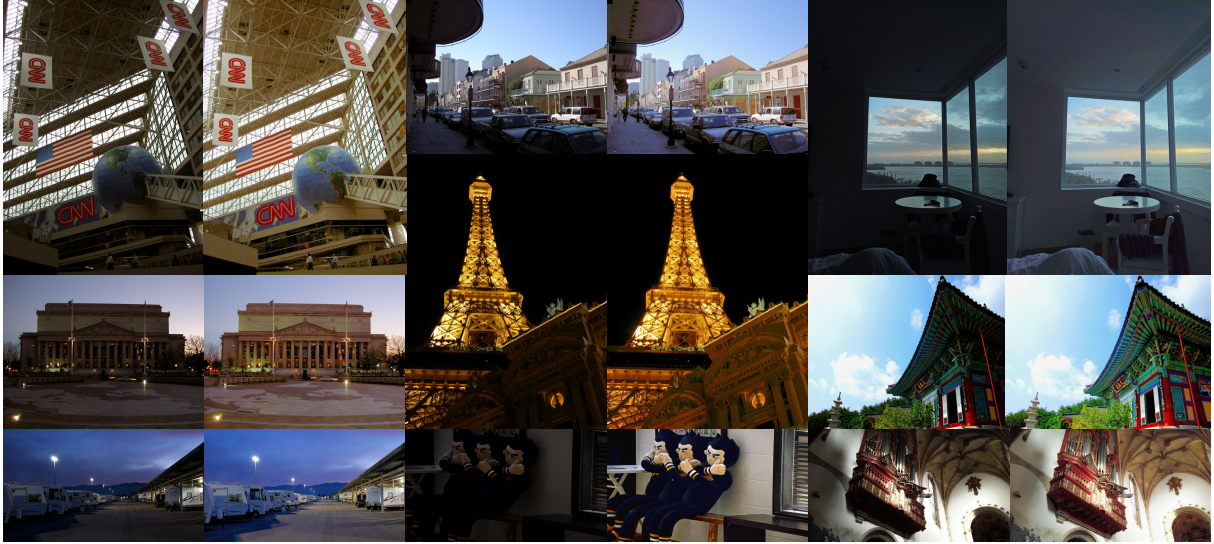


Fig. 1: Example of enhancing images in low-light environments using the ALEN method across different scenarios.

methods, from traditional approaches to advanced deep learning techniques. In this section, related works are categorized according to the different processing techniques used.

2.1 Histogram equalization-based methods

Classical methods, such as histogram adjustment and equalization [11, 12], have been fundamental in enhancing the visibility of images under low-light conditions. One of the first approaches was developed in 2007, Ibrahim et al. [31] proposed the Brightness Preserving Dynamic Histogram Equalization (BPDHE), a method that uses a Gaussian filter to smooth the input histogram and then applies equalization over segments defined by local maxima, preserving the mean brightness of the original image. That same year, Abdullah-Al-Wadud et al. [32] introduced Dynamic Histogram Equalization (DHE), a histogram equalization-based technique that enhances low-light images by dividing the histogram into segments based on local minima, assigning them specific ranges of grayscale levels, and verifying their redistribution to prevent dominance.

Later in 2013, Hitam et al. [33] introduced the so-called Contrast Limited Adaptive Histogram Equalization (CLAHE), a method specifically designed to enhance underwater images.

This approach applies CLAHE to RGB and HSV color models, combining the results using the Euclidean norm. More recently, in 2022, Thepade et al. [34] introduced an innovative fusion combining the CLAHE with BPDHE along with a linearly weighted color restoration technique. The next year, in 2023, Han et al. [35] proposed the Histogram Equalization–Multiscale Retinex Combination (HE-MSR-COM) method, which consists of three main modules: MSR enhancement for edges, HE enhancement for illumination, and frequency domain fusion. This approach adapts edge and illumination information using derived weights for different scenarios.

2.2 Retinex-based methods

Retinex theory [36] enhances visual perception by adjusting the color space through techniques that optimize dynamic range and color fidelity, especially under varying lighting conditions. [37, 38]

In 2016, Guo et al. [27] introduced the Low-light Image Enhancement via Illumination Map Estimation (LIME) method, which individually estimates the illumination of each pixel in a low-light image, refines this illumination map and applies it to enhance the image quality. A few years later, in 2018, Wei et al. [39] proposed Retinex-Net, which consists of two sub-networks: Decom-Net, for the decomposition of the image

into reflectance and illumination, and EnhanceNet, to adjust the illumination and improve the image quality. In 2022, Wu et al. [40] presented the URetinex method, which includes three key modules: initialization, unfolded optimization, and illumination adjustment. These modules allow the image to be decomposed into reflectance and illumination, adapting the results to suppress noise and preserve details.

The following year, in 2023, Yi et al. [41] introduced the Diff-Retinex method, which proposes a generative diffusion model for low-light image enhancement. It uses a Retinex Transformer Decomposition Network (TDN) to decompose the image into illumination and reflectance maps. That same year, Cai et al. [42] presented Retinexformer for enhancing low-light images and restoring corruptions using Retinex theory. They also developed an Illumination-Guided Transformer (IGT) for modeling non-local interactions under varying lighting conditions. Recently this year, in 2024, Bai et al. [43] proposed RetinexMamba, combining traditional Retinex methods' intuition with advanced deep learning techniques from Retinexformer. It improves processing speed with State Space Models (SSMs) and introduces new illumination estimators and restoration mechanisms while enhancing model interpretability with a Fused Attention mechanism.

2.3 Unsupervised and self-calibrated approaches

Unsupervised approaches, such as self-calibrated methods, enhance low-light images by automatically adjusting parameters to optimize their visual quality.

In 2019, Zhang et al. [44] introduced a method that improves images through dual illumination estimation. It separately corrects underexposed and overexposed parts and then adaptively merges visually better-exposed parts from multiple images to create a well-exposed single image. In 2021, Zhang et al. [45] proposed a method that uses a Histogram Equalization Prior (HEP) to guide the process. This unsupervised learning process is divided into two modules: Light Up Module (LUM) and Noise Disentanglement Module (NDM).

Later in 2022, Jin et al. [46] presented an unsupervised method for enhancing night images

using layer decomposition and light-effects suppression. In the same year, Ma et al. [47] introduced SCI, employing cascaded learning with weight sharing to reduce computational cost and adapt to various scenes through unsupervised training. In 2023, Liang et al. [48] proposed the Contrastive Language-Image Pre-Training (CLIP-LIT), a method that utilizes CLIP to distinguish between backlit and well-lit images. It improves the network through a prompt-based learning framework that optimizes text-image similarity.

More recently, in 2024, Chen and Yu [49] proposed the Unsupervised Reflectance Retinex and Noise model (URRN-Net) to enhance low-light construction images. It addresses challenges like uneven lighting and noise using CNNs to decompose lighting features and restore brightness through unsupervised loss functions. On the other hand, Xu et al. [50] introduced Degraded Structure and Hue Guided Auxiliary Learning (SHAL-Net), an unsupervised method that utilizes auxiliary learning guided by the degraded structure and tone of the image.

2.4 Deep learning-based methods

Deep Learning methods yield favorable generalization results based on the quantity and quality of input images. In 2020, Wang et al. [51] presented Deep Lightning Network (DLN), which uses Lightning Back-Projection (LBP) blocks to iteratively adjust the illumination and Feature Aggregation (FA) blocks to adaptively merge results. During that same year, Guo et al. [52] proposed the Zero-reference Deep Curve Estimation (Zero-DCE) method, which enhances lighting using the deep network DCE-Net. This network adjusts specific image curves and employs non-reference loss functions to guide learning.

The following year, in 2021, Liu et al. [53] proposed the Retinex-Inspired Unrolling With Cooperative Prior Architecture Search architecture, which models the intrinsic structure of underexposed images and develops optimization processes to construct a comprehensive propagation structure. On the other hand, in the same year, Zheng et al. [54] introduced the Adaptive Unfolding Total Variation Network (UTVNet) architecture, which estimates noise level and learns a corresponding map through total variation regularization.

Guided by this map, UTVNet effectively recovers fine details and suppresses noise.

Later in 2022, Fan et al [55] introduced HWM-Net, an image enhancement network based on the enhanced hierarchical model M-Net+. This network uses a half wavelet attention block to enrich wavelet domain features. Within the same year, Wang et al. [56] proposed a method using a normalizing flow model to enhance low-light images towards normal exposure. This approach employs an invertible network that adjusts low-light images to map them to a Gaussian distribution of normally exposed images. On the other hand, Cui et al. [57] presented a lightweight and fast Adaptive Lighting Transformer (IAT) to restore normal sRGB images from low-light, underexposed, or overexposed conditions.

More recently, in 2023, Ma et al. [58] introduced a method to enhance images in low-light scenes using a learning approach that explores relationships between different scenes. They used a bi-level learning framework to optimize hyperparameters and improve the encoder’s adaptability to diverse scenes. In the same year, Guo and Hu [59] proposed a method that converts RGB images to luminance-chrominance. It uses an adjustable noise suppression network to enhance luminance, guided by a lighting map to control noise amplification. Finally, Fu et al. [60] proposed PairLIE, an approach that learns adaptive prior values from pairs of low-light images.

3 Materials and Methods

In this section the datasets used and generated are presented, the ALEN design criterion and its modules are described, and experimental details are detailed.

3.1 Datasets

Four different datasets are used in this proposal: the custom-developed Global-Local Illumination (GLI) dataset is designed for illumination classification. For the estimation part, two public datasets are employed for illumination estimation, and one specific dataset is used for color estimation. These datasets are described in detail below.

3.1.1 Dataset for illuminance classification

A key challenge in the proposed framework is developing a dataset to distinguish between images needing global or local enhancement. Due to the lack of a suitable dataset, a new dataset called GLI was constructed from multiple public databases focused on low-light image enhancement. Each dataset offers unique features for estimating image enhancement under these conditions. The primary goal is to identify illumination variations and common features, creating a classification dataset.

During the initial stages of creating the GLI dataset, each image undergoes visual inspection and classification from a human perspective to determine whether global or local enhancement is required. To aid in this process, histograms of various image types are analyzed to evaluate illumination uniformity. Analyzing histograms is essential for understanding how pixel intensities are distributed in low-light images. Pixel intensity is assessed individually for each channel in RGB-format images, ranging from 0 to 255. Based on the histogram analysis shown in Fig. 2, a detailed representation of intensity value distributions is provided. Figure 2a shows an example of an image requiring global enhancement from the LOL [39] dataset, while Fig. 2b presents the histogram of an image requiring local enhancement taken from the DICM [26] dataset.

Through this analysis, it can be inferred that images requiring global enhancements predominantly exhibit pixel intensities on the left side of the histogram, resulting in decreased values on the right side. Conversely, images needing local enhancements display intensity values covering the entire histogram range, focusing mainly on the extremes near the road and tree zones.

In the second stage of creating the GLI dataset, after the human visual inspection, images are converted to grayscale, marking the beginning of parameter-based classification to determine whether an image belongs to the local or global category. For any grayscale image I , the histogram $Hist(i)$ is computed by quantifying a pixel according to their respective intensity levels. This can be mathematically expressed as:

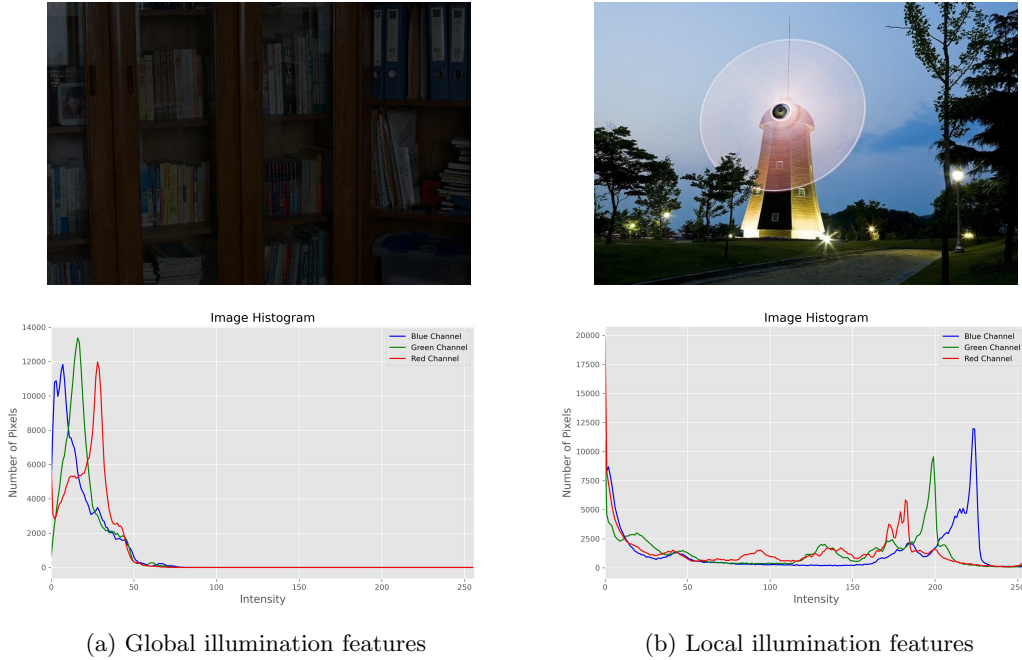


Fig. 2: Comparison of global and local illumination features.

$$Hist(i) = \sum_{p=0}^{255} \delta(I(p), i) \quad (1)$$

where δ is a function derived from the Kronecker delta function. Its output is 1 if its two parameters are equal and 0 otherwise. Therefore, if the intensity of pixel p is equal to i , $\delta(I(p), i)$ returns 1; otherwise, it returns 0. By summing these values for all pixels in the image, the count of pixels displaying intensity i is obtained. The threshold defining the image category labels is mathematically set as follows:

$$I_{thr} = \max\{i \mid Hist(i) \geq T\} \quad (2)$$

where $Hist(i)$ denotes the count of pixels with intensity i , while T represents the predefined threshold for image classification. According to Eq. 2, I_{thr} represents the sought threshold intensity, crucial for distinguishing whether an image is classified as global or local. A total of 2000 images were used, divided into two main categories: 1000 images labeled as “global” and another 1000 as “local”. Figure 3a shows an example of “global” labeled images from the LOL dataset, while Fig. 3b presents an example of “local” labeled images from the DICM dataset.



Fig. 3: Example images from the training set for classification.

3.1.2 Datasets for illuminance and color estimation

The illumination estimation sections of the proposed method use two specific datasets: HDR+ [61] for global illumination enhancement and Synthetic Low-Light (SLL) [62] for local illumination enhancement, while the color estimation section employs the MIT-Adobe FiveK [63]. HDR+ dataset [61] used for global illumination enhancement consists of 3640 scenes, each with

2 to 10 photos in their original format. Specifically, the version selected by Zeng et al. [64] was used, which includes 922 paired photos of low and normal illumination.

Synthetic Low-Light (SLL) dataset [62] is generated from original images of public datasets such as COCO [65] or ImageNet [66]. This dataset employs strategies including gamma adjustments, reduced dynamic range to simulate loss of detail in dark areas, and the addition of various types of noise to replicate low-light conditions. Additionally, SLL provides multiple exposure levels (original, 1/4x, 1/8x, 1/16x, and 1/32x) to enhance generalization. This dataset, comprising 22,656 paired training images and 965 paired test images, is specifically designed to improve local illumination.

Finally, the MIT-Adobe FiveK dataset [63] consists of 5,000 paired images, each enhanced by five different experts. This dataset balances improvements in global and local illumination, achieving a more vivid and realistic color restoration. Figure 4 presents the three aforementioned datasets used to train the lighting and color estimation sections. The first row displays the original images to be enhanced, while the second row showcases reference images representing the ideal versions sought through the enhancement process.



Fig. 4: Example images from the training set for estimation.

3.2 ALEN Design

In recent studies, various methods have been employed to enhance low-light images, including CNNs, GANs, Transformer-based architectures, and statistical methods. The performance of each method varies depending on the image capture conditions and the training dataset, especially for

neural network-based approaches. However, the adaptability of these algorithms does not always guarantee consistent improvement across different datasets. Therefore, the proposed method, ALEN, addresses this diversity by combining multiple neural network designs. Figure 5 illustrates the overall structure of the proposed ALEN architecture.

Based on the diagram shown in Fig. 5, various sections can be identified that encompass different aspects of the comprehensive architecture aimed at enhancing low-light images. The main components of the diagram include the classifier (C_L), Global Enhancement (G_E), Local Enhancement (L_E), and Color Enhancement (C_E).

Considering H and W the height and width of the image in pixels, respectively, C_L analyzes the images $\mathbf{I}_{low} \in \mathbb{R}^{H \times W \times 3}$ to determine whether to apply global enhancement, represented by $\mathbf{I}_G \in \mathbb{R}^{H \times W \times 3}$, or local enhancement, represented by $\mathbf{I}_L \in \mathbb{R}^{H \times W \times 3}$. C_L relies on Light Classification Network (LCNet), a lightweight classification sub-network that extracts image features and determines the necessary enhancement type based on these features.

For the estimation of G_E , L_E , and C_E , the Single-Channel Network (SCNet) and Multi-Channel Network (MCNet) sub-networks are used. SCNet employs a single channel of information for illumination enhancement, specifically the V channel in the HSV color space. On the other hand, MCNet allows for the independent extraction of information from each channel in the RGB color space. For G_E , a global input image \mathbf{I}_G is considered. The process begins with the conversion from RGB to HSV and the extraction of the V channel from \mathbf{I}_G . Subsequently, this V channel extraction is processed by the SCNet sub-network. This procedure can be mathematically expressed in Eqs. 3 and 4, respectively.

$$\mathbf{V}_G = \mathcal{T}_{HSV}(\mathbf{I}_G[R], \mathbf{I}_G[G], \mathbf{I}_G[B])[V] \quad (3)$$

$$\mathbf{V}'_G = \text{SCNet}(\mathbf{V}_G) \quad (4)$$

where $\mathbf{V}_G \in \mathbb{R}^{H \times W}$ represents the output of the channel extraction, \mathcal{T}_{HSV} denotes the RGB to HSV transformation function, $[\cdot]$ indicates channel extraction, and V is the specific channel extracted from this conversion. Following that, in Eq. 4,

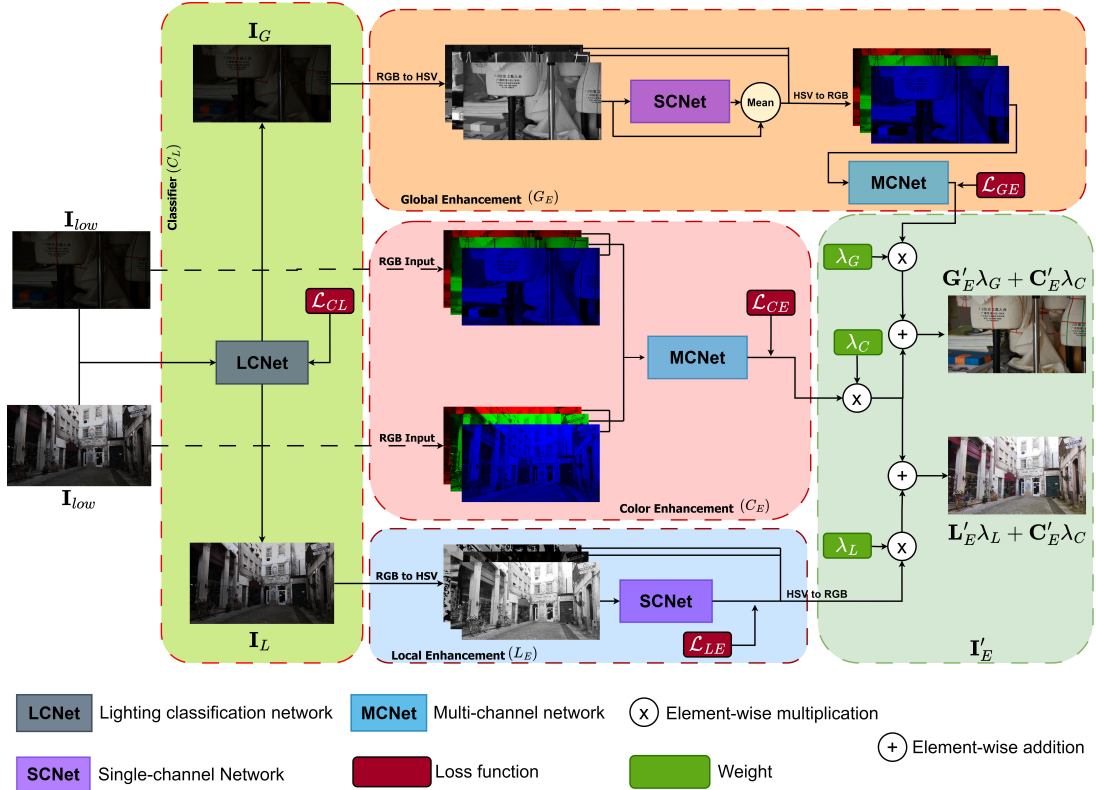


Fig. 5: The architecture of the proposed method.

$\mathbf{V}'_G \in \mathbb{R}^{H \times W}$ represents the output of the channel processed by the SCNet sub-network. Continuing with the process, \mathbf{V}_G and \mathbf{V}'_G are averaged to preserve the characteristics of the V channel. Then, the conversion from HSV to RGB is performed, which is expressed as follows:

$$\mathbf{I}'_G = \mathcal{T}_{\text{RGB}} \left(\mathbf{I}_G[H], \mathbf{I}_G[S], \frac{\mathbf{V}_G + \mathbf{V}'_G}{2} \right) \quad (5)$$

where $\mathbf{I}'_G \in \mathbb{R}^{H \times W \times 3}$ stands for the output of the conversion using the averages of $\mathbf{V}_G + \mathbf{V}'_G$ and \mathcal{T}_{RGB} is the transformation function from HSV to RGB. Finally, to obtain the global illumination enhancement in each of its RGB channels, it is passed through MCNet, which allows independent enhancement of information in each channel of the RGB color space. This can be expressed mathematically as:

$$\mathbf{G}'_E = \text{MCNet}(\mathbf{I}'_G[R], \mathbf{I}'_G[G], \mathbf{I}'_G[B]) \quad (6)$$

where $\mathbf{G}'_E \in \mathbb{R}^{H \times W \times 3}$ denotes the output obtained after passing \mathbf{I}'_G through MCNet.

In the case of L_E , the input image is \mathbf{I}_L . For \mathbf{I}_L to be processed by the SCNet sub-network, it must first be transformed from RGB to HSV. This transformation allows for the extraction and specific processing of the V channel.

The complete process, from the transformation to the processing by SCNet, is detailed in Eqs. 7 and 8.

$$\mathbf{V}_L = \mathcal{T}_{\text{HSV}}(\mathbf{I}_L[R], \mathbf{I}_L[G], \mathbf{I}_L[B])[V] \quad (7)$$

$$\mathbf{V}'_L = \text{SCNet}(\mathbf{V}_L) \quad (8)$$

where $\mathbf{V}_L \in \mathbb{R}^{H \times W}$ represents the extraction of the V channel from the HSV color space, and \mathcal{T}_{HSV} is the transformation function from RGB to HSV. On the other hand, $\mathbf{V}'_L \in \mathbb{R}^{H \times W}$ is the output obtained after passing \mathbf{V}_L through the SCNet sub-network. After this processing, \mathbf{V}'_L is converted

back to the RGB color space to obtain the final output of the local illumination enhancement.

This process is expressed as follows:

$$\mathbf{L}'_E = \mathcal{T}_{\text{RGB}}(\mathbf{I}_L[H], \mathbf{I}_L[S], \mathbf{V}'_L) \quad (9)$$

where $\mathbf{L}'_E \in \mathbb{R}^{H \times W \times 3}$ represents the output of the local illumination enhancement and \mathcal{T}_{RGB} is the transformation from HSV to RGB. For C_E , the images \mathbf{I}_{low} are considered as input. In this process, \mathbf{I}_{low} is fed directly into the MCNet sub-network without passing through the classifier, allowing for color enhancement based on the primary characteristics of the input images.

This can be expressed mathematically as follows:

$$\mathbf{C}'_E = \text{MCNet}(\mathbf{I}_{low}[R], \mathbf{I}_{low}[G], \mathbf{I}_{low}[B]) \quad (10)$$

where $\mathbf{C}'_E \in \mathbb{R}^{H \times W \times 3}$ is the resulting image with color enhancement.

Finally, the combination of the local and global enhancement processes with the color enhancement of the image can be expressed as follows:

$$\mathbf{I}'_E = \begin{cases} \mathbf{G}'_E \lambda_G + \mathbf{C}'_E \lambda_C & \text{Global enhancement} \\ \mathbf{L}'_E \lambda_L + \mathbf{C}'_E \lambda_C & \text{Local enhancement} \end{cases} \quad (11)$$

where $\mathbf{I}'_E \in \mathbb{R}^{H \times W \times 3}$ represents the enhanced image, whether locally or globally, \mathbf{G}'_E denotes the global illumination enhancement, \mathbf{L}'_E is the local illumination enhancement, and \mathbf{C}'_E stand for color enhancement. On the other hand λ_G , λ_L , and λ_C are corresponding weights used to achieve the optimal fusion between the images.

To provide a more precise description of the ALEN architecture, the LCNet, SCNet, and MCNet sub-networks for light classification and estimation, as well as image color, are detailed first, covering Sections 3.2.1 and 3.2.2. These sections delve into the key elements of the required convolutional layers, including the core concepts of executing the proposed model. Subsequently, Section 3.2.3 thoroughly describes the loss functions used to achieve the desired model outcomes, which are employed in the models developed in Sections 3.2.1 and 3.2.2. This step-by-step analysis provides a deeper understanding of the neural network architectures required for light classification and estimation, as well as image color training.

3.2.1 Classification architecture

LCNet extracts image features and determines whether global or local improvement is needed using a binary classifier. The network includes two convolutional blocks and two fully connected layers. Each convolutional block consists of convolution operations, ReLU activation, and max pooling (MaxPool). The first block applies 32 convolution filters of size 3x3 to the three-channel input image (RGB), with a stride of 1 and padding of 1, followed by max pooling to halve the spatial dimensions. The second block uses 64 convolution filters and another max pooling layer. The output is then flattened and fed into the fully connected layers. The first fully connected layer reduces features to 128 dimensions, applies ReLU activation, and includes a dropout layer with a 0.5 probability to prevent overfitting. The final fully connected layer reduces the dimensions from 128 to 2. The network’s forward function processes input data through these layers to produce outputs, with each output being a vector of length 2, representing scores for two classes (global or local improvement). Table 1 details the values in LCNet construction.

Table 1: Characteristics of LCNet.

Layer	Input	Output	Filter Kernel	Stride	Padding
Feature Extraction					
Conv 1	3	32	3x3	1	1
Pool 1	32	32	2x2	2	0
Conv 2	32	64	3x3	1	1
Pool 2	64	64	2x2	2	0
Flat 1	64*56*56	128	-	-	-
Flat 2	128	2	-	-	-

3.2.2 Estimation architectures

SCNet begins with three consecutive convolutional layers, each followed by ReLU activation, doubling the output channels at each layer up to 128. A fourth convolutional layer with ReLU activation increases the channels to 256. The fifth layer reduces the output to 128 channels, and its output is concatenated with the third layer’s output to form a skip connection, preserving previous features. The sixth layer reduces the channels to 64 and is concatenated with the second layer’s



Fig. 6: Visual comparison of methods for enhancing low-light images on DICM and LIME datasets.

output, creating another skip connection. The seventh layer reduces the channels to 32, and its output is concatenated with the first layer’s output, forming a third skip connection. Finally, an eighth layer reduces the output dimensions to the original input size. SCNet does not include pooling or fully connected layers; instead, it focuses on convolution and feature combination through skip connections to retain information from earlier layers. Table 2 details each convolutional layer and the convolutional kernels used.

MCNet begins with feature extraction and filter reduction. An initial 3x3 convolutional layer extracts basic features with stride and padding of 1. Several subsequent 3x3 convolutional layers (Conv 1-6) deepen the features and reduce the number of filters. The final layer (Final) uses 1x1 filters to reduce the output to a single channel,

Table 2: Characteristics of SCNet.

Layer	Input	Output	Filter Kernel	Stride	Padding
Feature Extraction					
Conv 1	1	32	3x3	1	1
Conv 2	32	64	3x3	1	1
Conv 3	64	128	3x3	1	1
Conv 4	128	256	3x3	1	1
Filter Reduction					
Conv 5	256	128	1x1	1	0
Conv 6	256	64	1x1	1	0
Conv 7	128	32	1x1	1	0
Conv 8	64	1	1x1	1	0

compressing the information. MCNet also includes a channel adjustment phase, where Conv 1 and Conv 2 use 1x1 filters for channel dimension transformation. A fusion convolutional layer (Conv Fusion) with 3x3 filters merges multi-channel features. Most layers use ReLU activation, while the

fusion layer uses the Sigmoid function to normalize the output to a range of 0 to 1. Table 3 details each convolutional layer and the convolutional kernels used.

Table 3: Characteristics of MCNet.

Layer	Input	Output	Filter Kernel	Stride	Padding
Channel Adjustment					
Conv 1	32	64	1x1	1	0
Conv 2	64	128	1x1	1	0
Feature Extraction/Filter Reduction					
Initial	1	32	3x3	1	1
Conv 1	32	32	3x3	1	1
Conv 2	32	64	3x3	1	1
Conv 3	64	64	3x3	1	1
Conv 4	64	128	3x3	1	1
Conv 5	128	64	3x3	1	1
Conv 6	32	32	3x3	1	1
Final	32	1	1x1	1	0
Conv Fusion	3	3	3x3	1	1

3.2.3 Loss functions

The overall design of the model is based on two fundamental structures encompassing classification and estimation aspects for low-light images. This design is divided into four independent sub-processes. Although the entire architecture focuses on the classifier’s decisions, it is essential to consider certain criteria to optimize the performance of each proposed design. A key criterion is the loss function, which measures the difference between the model’s predictions and the actual values. During training, the main objective is to minimize the loss function by adjusting the model’s parameters. In the proposed architecture, four different loss functions are employed, offering significant potential for improvement in low-light images.

Loss function for illuminance classification. For the classification network, the Binary Cross-Entropy (BCE) [67] loss function will be used, specifically tailored for binary classification problems. This function measures the difference between two probability distributions: the probability distribution of true labels and the probability distribution predicted by the model. It is mathematically expressed as follows:

$$\mathcal{L}_{CL}(\hat{y}_i, y_i) = -\frac{1}{N} \sum_{i=0}^N \left[y_i \cdot \log(\hat{y}_i) + (1 - y_i) \cdot \log(1 - \hat{y}_i) \right] \quad (12)$$

where N is the batch size of low-light images, y_i represents the actual label, indicating whether the image needs global or local illumination enhancement. On the other hand, \hat{y}_i denotes the predicted probability of the category, ranging from 0 to 1. The function $\log(\cdot)$ converts probabilities to the natural logarithm scale. The term $y_i \cdot \log(\hat{y}_i)$ corresponds to the global category, while $(1 - y_i) \cdot \log(1 - \hat{y}_i)$ refers to the local category.

Loss functions for image enhancement.

For the estimation part, it is divided into three sections: \mathcal{L}_{LE} for local illumination enhancement, \mathcal{L}_{GE} for global illumination enhancement, and \mathcal{L}_{CE} for image color enhancement. The first section focused on local illumination enhancement (\mathcal{L}_{LE}) and aims to preserve the structure of the image. Therefore, the loss function in this case is:

$$\mathcal{L}_{LE} = \mathcal{L}_s \quad (13)$$

On the other hand, in the second section, the target is to enhance global illumination (\mathcal{L}_{GE}), for which three loss components are combined: contrast (\mathcal{L}_c), structure (\mathcal{L}_s), and perceptual (\mathcal{L}_p). The complete loss function is defined as:

$$\mathcal{L}_{GE} = \mathcal{L}_c + \mathcal{L}_s + \mathcal{L}_p \quad (14)$$

In the third section, which addresses the enhancement of color contrast (\mathcal{L}_{CE}), the same loss components are combined: contrast (\mathcal{L}_c), structure (\mathcal{L}_s), and perceptual (\mathcal{L}_p). The complete loss function for this purpose is defined as:

$$\mathcal{L}_{CE} = \mathcal{L}_c + \mathcal{L}_s + \mathcal{L}_p \quad (15)$$

The loss components of \mathcal{L}_c , \mathcal{L}_s and \mathcal{L}_p is mathematically expressed as follows:

$$\mathcal{L}_c(\hat{y}, y) = \frac{1}{N} \sum_{i=1}^n (y - \hat{y})^2 \quad (16)$$

$$\mathcal{L}_s(\hat{y}, y) = 1 - \frac{(2\mu_{\hat{y}}\mu_y + c_1)(2\sigma_{\hat{y}y} + c_2)}{(\mu_{\hat{y}}^2 + \mu_y^2 + c_1)(\sigma_{\hat{y}}^2 + \sigma_y^2 + c_2)} \quad (17)$$

$$\mathcal{L}_p = \frac{1}{N} \sum_{i=1}^N \frac{1}{C_j H_j W_j} \|\phi_j(\hat{y}) - \phi_j(y)\|_2^2 \quad (18)$$

For the loss component \mathcal{L}_c , it is computed using the Mean Squared Error (MSE) function [68]. Here, \hat{y} represents the model’s prediction, y is the ground truth of the reference image, and N is the total number of pixels.

On the other hand, the loss component \mathcal{L}_s is based on the Structural Similarity Index Measure (SSIM) [69]. Here, \hat{y} and y represent the two images being compared, $\mu_{\hat{y}}$ and μ_y denote the mean of the images \hat{y} and y , respectively. Additionally, $\sigma_{\hat{y}}$ and σ_y represent the variance of images \hat{y} and y , while $\sigma_{\hat{y}y}$ denotes the covariance between images \hat{y} and y . To prevent division by zero, constants C_1 and C_2 are introduced as small values.

Finally, the loss component \mathcal{L}_p utilizes features extracted from the VGG network [70, 71]. Here, N represents the total number of elements in the dataset, C_j , H_j , and W_j represent the number of channels, height, and width, respectively, in the j -th layer extracted by the VGG network. $\phi_j(\hat{y})$ and $\phi_j(y)$ correspond to the features extracted by the VGG network from the enhanced and reference images, respectively, at the j -th layer.

3.3 Implementation Details

Each network dedicated to classification, local and global illumination estimation, and color enhancement underwent separate training processes. PyTorch [72], an open-source machine learning library based on Torch known for its efficiency in training complex architectures, facilitated the implementation. The training took place on a PC equipped with an NVIDIA RTX 3060 GPU, an Intel Core i5-12400F CPU (running at 2.50GHz), and 16 GB of RAM.

For the classification network, the training involved 150 epochs using batches of 32 images resized to 224×224 pixels. The Adam optimizer [73] was employed with a learning rate set to 1e-3. A total of 1800 images from the GLI Dataset were used for training, with an additional 200 reserved for testing. The local illumination estimation network underwent 500 epochs of training using batches of 8 images at 224×224 pixels resolution.

The training also utilized the Adam optimizer with a learning rate of 1e-3, leveraging the SLL dataset comprising 22,472 image pairs.

Similarly, the global illumination estimation network was trained for 40 epochs with batches of 8 images, randomly selecting 128×128 blocks from each image. The Adam optimizer with a learning rate of 1e-3 was applied, reducing the rate by half after 20 epochs. The training utilized the custom HDR+ dataset containing 922 image pairs. Lastly, the color enhancement network underwent 40 epochs of training with batches of 8 images, randomly selecting 128×128 blocks. The Adam optimizer with a learning rate of 1e-4, reduced by half after 20 epochs, was employed. Training data came from the MIT-Adobe FiveK dataset, comprising 5000 image pairs.

4 Results and Discussions

To assess the performance of the proposed method ALEN, it was compared against a series of state-of-the-art methods, including LIME (Guo et al.) [27], RetinexNet (Wei et al.) [39], DUAL (Zhang et al.) [44], Zero-DCE (Guo et al.) [52], RUAS (Liu et al.) [53], UTVNet (Zheng et al.) [54], HWMNet (Fan et al.) [55], LLFlow (Wang et al.) [56], SCI (Ma et al.) [47], IAT (Cui et al.) [57], BL (Ma et al.) [58], Bread [74], PairLIE (Fu et al.) [60], CLIP-LIT (Liang et al.) [48], SHAL-Net (Jiang et al.) [50], and GSAD [75]. These methods are available for research, enabling their performance to be compared with the proposed method.

4.1 Quantitative results

To evaluate the efficiency of the proposed ALEN method alongside other state-of-the-art methods, Full-Reference IQA (FIQA) and No-Reference IQA (NIQA) metrics were employed. FIQA metrics require reference images for measurements, including Peak Signal-to-Noise Ratio (PSNR) [69], Structural Similarity Index Measure (SSIM) [69], Universal Quality Index (UQI) [76], Learned Perceptual Image Patch Similarity (LPIPS) [77], and DeltaE [50]. In contrast, NIQA metrics such as Naturalness Image Quality Evaluator (NIQE) [78] do not rely on a reference image. The evaluation included 735 images from the UHD-LOL4k [79] dataset and 735 images from the Large-Scale



Fig. 7: Visual comparison of methods for enhancing low-light images on MEF and NPE datasets.

Real-Word (LSRW) [80] dataset. Table 4 presents the results of these assessments using different datasets and metrics, where \uparrow indicates higher values are better and \downarrow indicates lower values are better.

In Table 4, compared with other methods, the proposed method ALEN demonstrated outstanding performance. In the UHD-LOL4K dataset, ALEN achieved a PSNR of 22.0211, SSIM of 0.9283, UQI of 0.9463, NIQE of 5.0931 and LPIPS of 0.0380. Although methods such as HWMNet, LLFlow, CLIP-LIT, and GSAD showed acceptable performance on this dataset, the proposed method clearly outperformed them. On the other hand, RUAS and SCI exhibited poor performance on the UHD-LOL4K dataset. For the LSRW dataset, the consistent and outstanding performance of

the proposed method is evident. ALEN reached a PSNR of 18.2588, SSIM of 0.6746, UQI of 0.8293, NIQE of 2.7373, LPIPS of 0.2048, and DeltaE of 14.3309, surpassing all other methods evaluated on this dataset. Conversely, Bread, PairLIE, HWMNet, GSAD and Zero-DCE showed acceptable results, while RUAS and BL exhibited poor performance on this dataset.

In another evaluation quantitative, the datasets real-world scenes DICM [26], LIME [27], MEF [28], NPE [29], and DIS were considered. These datasets, being unpaired, lack a reference image for evaluation, and thus were solely assessed using the NIQE metric. Table 5 presents the results of the comprehensive evaluation of the aforementioned datasets, where \downarrow indicates that a lower value is better.

Table 4: Comparison results on UHD-LOL4K and LSRW datasets in terms of PSNR, SSIM, NIQE, UQI, LPIPS and DeltaE. The bold highlights the best result.

Method	Year	UHD-LOL4K Dataset						LSRW Dataset					
		PSNR \uparrow	SSIM \uparrow	NIQE \downarrow	UQI \uparrow	LPIPS \downarrow	DeltaE \downarrow	PSNR \uparrow	SSIM \uparrow	NIQE \downarrow	UQI \uparrow	LPIPS \downarrow	DeltaE \downarrow
LIME [27]	2016	18.5128	0.8784	5.9088	0.9059	0.0868	12.8371	15.8357	0.5673	3.7173	0.7437	0.3241	20.0141
RetinexNet [39]	2018	15.6315	0.8142	6.5863	0.8507	0.1384	18.6405	15.3022	0.4718	4.6158	0.7415	0.4238	21.4150
DUAL [44]	2019	18.9064	0.8761	5.6354	0.9232	0.0847	12.6130	14.9926	0.5682	3.5961	0.7127	0.3169	22.7693
Zero-DCE [52]	2020	19.9615	0.8436	5.7367	0.9233	0.0501	11.7076	17.1099	0.6251	3.6593	0.7943	0.2529	16.2985
RUAS [53]	2021	14.7100	0.7052	7.0241	0.8757	0.1594	15.8462	14.8709	0.5840	3.4300	0.7584	0.2862	17.3777
UTVNet [54]	2021	15.8912	0.6265	5.5775	0.8858	0.1441	15.4056	17.4206	0.6075	3.5366	0.8101	0.2163	17.1897
HWMNet [55]	2022	19.0511	0.8692	5.5613	0.9284	0.0813	11.5452	17.1721	0.6622	3.2333	0.8141	0.2186	17.2823
LLFlow [56]	2022	19.2917	0.8828	5.3948	0.9282	0.0677	11.7015	17.1178	0.6233	2.8918	0.8105	0.2452	16.8416
SCI [47]	2022	13.4004	0.7027	6.1473	0.8345	0.1668	19.9549	17.1191	0.5852	3.5260	0.7457	0.2446	17.8979
IAT [57]	2022	18.2540	0.8000	5.3895	0.9131	0.1208	13.5522	17.2690	0.6621	3.3039	0.7865	0.2222	18.1291
BL [58]	2023	15.8303	0.7611	6.7241	0.8859	0.1302	14.8801	13.2209	0.4580	3.2995	0.4695	0.2597	34.8050
Bread [74]	2023	18.5415	0.8706	5.3684	0.8877	0.0775	15.3285	16.4824	0.6702	3.1551	0.7854	0.2216	20.0266
PairLIE [60]	2023	15.9890	0.8104	5.7654	0.8507	0.1232	19.0069	17.8606	0.6359	3.1296	0.8102	0.2258	16.3977
CLIP-LIT [48]	2023	20.6842	0.9182	5.8932	0.9387	0.0604	10.6747	14.0537	0.5764	3.8504	0.6813	0.3146	24.9381
SHAL-Net [50]	2024	18.6282	0.7707	5.5736	0.9278	0.1361	11.6618	16.6353	0.5656	3.6336	0.7936	0.2701	17.4095
GSAD [75]	2024	21.2658	0.8657	5.1023	0.9365	0.1031	9.6162	17.4369	0.6298	3.4060	0.8146	0.2288	17.0808
ALEN (Proposed)	2024	22.0211	0.9283	5.0931	0.9463	0.0380	9.7990	18.2588	0.6746	2.7373	0.8293	0.2048	14.3309

Table 5: Comparison results on DICM, LIME, MEF, NPE and DIS datasets in terms of NIQE \downarrow . The bold highlights the best result.

Method	Year	DICM	DIS	LIME	MEF	NPE	Average
LIME [27]	2016	3.5345	3.2577	4.0482	3.4220	3.2599	3.5045
RetinexNet [39]	2018	4.3311	4.1928	5.3635	4.9390	3.5168	4.4686
DUAL [44]	2019	3.5733	3.2667	4.1015	3.5012	3.3670	3.5619
Zero-DCE [52]	2020	3.4540	3.2197	3.8189	3.2232	2.8970	3.3226
RUAS [53]	2021	5.0041	4.1015	4.2925	4.0922	6.4952	4.7971
UTVNet [54]	2021	3.9962	3.6354	3.7031	3.3070	3.7538	3.6791
HWMNet [55]	2022	3.2809	3.1222	3.8388	3.4695	3.4595	3.4342
LLFlow [56]	2022	3.3801	2.9456	3.9831	3.5434	3.6264	3.4957
SCI [47]	2022	3.6684	3.5215	4.1374	3.4398	3.8805	3.7295
IAT [57]	2022	3.6565	3.2308	4.1875	3.6588	3.6106	3.6688
BL [58]	2023	4.0940	3.9838	3.8805	3.3508	4.6247	3.9868
Bread [74]	2023	3.4036	3.2326	4.2077	3.6935	3.4443	3.5963
PairLIE [60]	2023	3.8209	3.3186	4.7434	3.9212	3.3467	3.8302
CLIP-LIT [48]	2023	3.7153	3.3942	4.0989	3.6041	3.1014	3.5828
SHAL-Net [50]	2024	3.6023	3.7415	3.9187	3.8450	3.7725	3.7760
GSAD [75]	2024	3.4803	3.2351	5.4784	3.6143	4.0690	3.9754
ALEN (Proposed)	2024	3.1811	2.9065	3.6926	3.1619	2.9734	3.1831

From the data provided in Table 5, it can be observed that the proposed method ranks first for the DICM, DIS, LIME, and MEF datasets with values of 3.1811, 2.9065, 3.6926, 3.1619, respectively. For the NPE dataset, the proposed method ranks second with a value of 2.9734. On the other hand, Zero-DCE exhibits the best performance for the NPE dataset. Overall, considering the average performance across all datasets, the proposed ALEN method achieves a score of 3.1831, surpassing all other methods and securing the first position, followed by the Zero-DCE method with a score of 3.3226.

4.2 Qualitative results

The qualitative evaluation includes images of various real-world scenes captured under low-light conditions. Figures 6, 7, and 8 depict images taken at different times of the day. Figure 6 presents day-time, twilight, and night-time scenes from the real-world image datasets DICM [26] and LIME [27]. Figure 7 displays images of day-time and twilight scenes from the MEF [28] and NPE [29] datasets, while Fig. 8 exhibits both day-time and night-time images from the proposed DIS dataset.

Regarding the enhancement of low-light images in day-time and twilight scenes, it is observed that methods such as SCI, IAT, BL, RUAS, HWMNet and SHAL-Net tend to over-illuminate, especially the sky portions of the

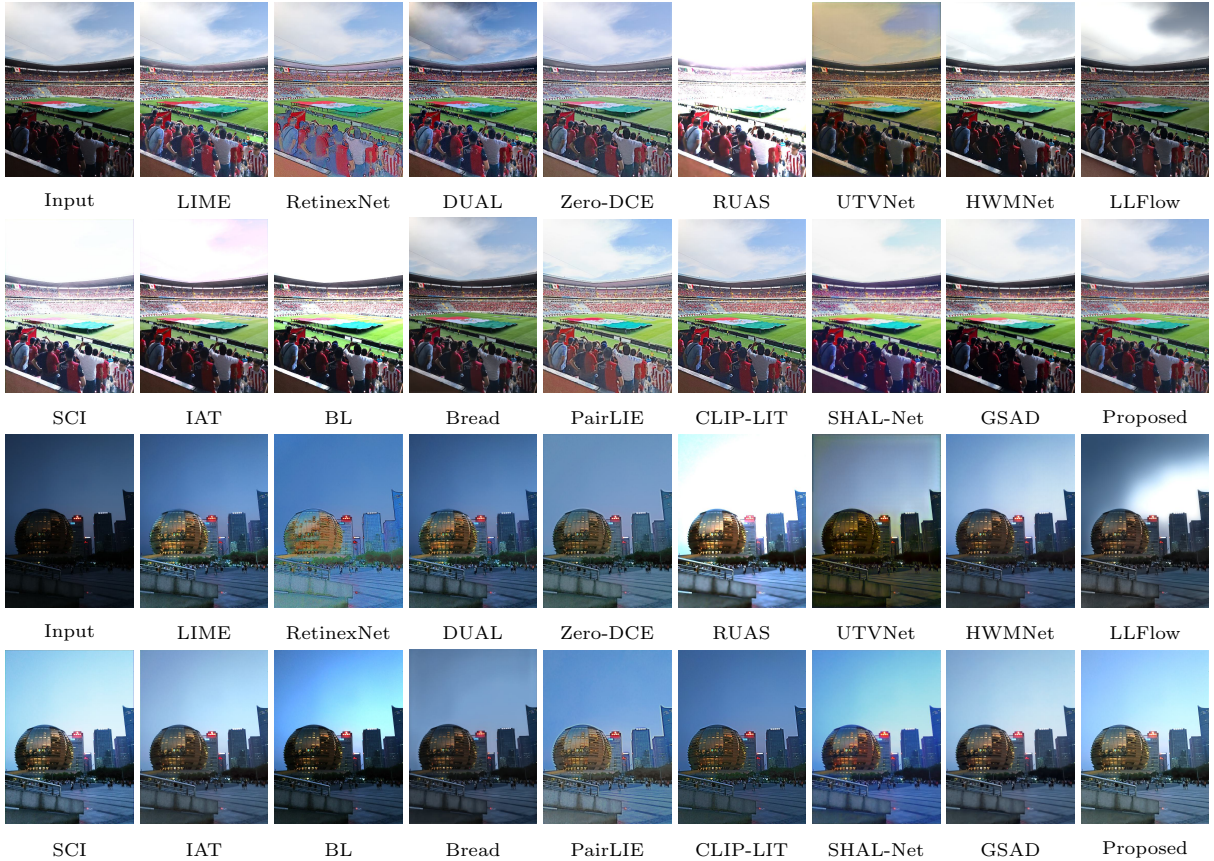


Fig. 8: Visual comparison of methods for enhancing low-light images on DIS dataset.

images. In contrast, methods like LLFlow and UTVNet exhibit color distortion, with UTVNet notably showing a yellowish tint. Methods such as CLIP-LIT, LIME, RetinexNet, and PairLIE, while achieving adequate illumination, introduce excessive color saturation, making the images appear unrealistic by overly highlighting the edges. Zero-DCE achieves good illumination but with noticeable color degradation. On the other hand, Bread and GSAD shows significant improvements in noise reduction, although the images remain slightly dark. DUAL enhances both illumination and color, but the edge highlighting is too prominent, affecting the perceived realism of the image. Finally, the proposed ALEN method stands out by achieving a good balance in illumination and color, demonstrating strong performance in both daytime and twilight scenes.

In the enhancement of night-time scene images, it is observed that methods such as

RUAS, HWMNet, SCI, IAT, and BL tend to over-illuminate certain areas of the images. Methods like RetinexNet, PairLIE, and SHAL-Net improve the images at the cost of color distortion. Methods such as Zero-DCE, UTVNet, and LLFlow achieve better illumination, but the resulting images exhibit muted colors. Visually, the methods LIME, DUAL, CLIP-LIT, Bread, GSAD, and the proposed ALEN offer the best results, with LIME, DUAL, and CLIP-LIT particularly excelling in highlighting image textures.

4.3 Ablation study

To evaluate the effectiveness of each module in the ALEN architecture, an ablation study was conducted examining the key components of the complete architecture: the Classifier (C_L), Local Enhancement (L_E), Global Enhancement (G_E), and Color Enhancement (C_E). These components are crucial for generating improved low-light

Table 6: Quantitative evaluation results of the ablation study on the performance of C_L , L_E , G_E , and C_E modules, evaluated using PSNR and SSIM metrics on UHD-LOL4K and LSRW dataset.

Model	Components				Metrics	
	C_L	L_E	G_E	C_E	PSNR	SSIM
Model w/o C_L and G_E		✓		✓	17.8703	0.7352
Model w/o C_L and L_E			✓	✓	16.0125	0.7014
Model w/o C_L , G_E and C_E		✓			16.6347	0.7229
Model w/o C_L , L_E and C_E			✓		18.0889	0.7487
Model w/o C_E	✓	✓	✓		18.9221	0.7985
Full Model	✓	✓	✓	✓	20.1399	0.8014

images in the proposed ALEN method. Table 6 presents the evaluation of each component in terms of the PSNR and SSIM metrics, assessed on a combined dataset containing 735 images from the UHD-LOL4K dataset and 735 images from the LSRW dataset mentioned in the quantitative results section. The results show that the complete model achieved the best performance, with a PSNR of 20.13 and an SSIM of 0.8014. This analysis highlights the importance of each module in the ALEN architecture.

4.4 Improving high-level vision tasks

A promising application of the proposed ALEN method as a preprocessing enhancement for low-light conditions is semantic segmentation. To evaluate this application, the Night-time Object Detection (NOD) dataset [81], which includes over 7,000 images and 46,000 annotated objects, was utilized. The impact of the ALEN method was assessed by implementing it as preprocessing before segmentation. For segmentation, the Segment Anything Model (SAM) [82] was employed. SAM features an image encoder based on a pre-trained Vision Transformer, a prompt encoder for multiple inputs, and a mask decoder for precise segmentation. Figure 9 shows a sample image from the NOD dataset, with the original low-light image and its segmentation results in the first column, and the enhanced image using the ALEN method and its segmentation results in the second column. The enhanced image shows better visibility and detail, leading to more accurate segmentation. These results demonstrate that applying the proposed method before SAM significantly improves image segmentation under low-light conditions.



(a) Original image and its (b) Enhanced image and its segmentation

Fig. 9: SAM-based segmentation analysis.

5 Conclusions and further work

This article introduces ALEN, a novel method specifically designed to enhance the visual quality of images captured under low-light conditions. By integrating global and local improvements through a lighting classification network and three convolutional estimator networks, ALEN has demonstrated its capability to significantly enhance both illumination and color in dark environments. This approach not only optimizes the perceptual quality of images and reduces noise but also facilitates advanced tasks in high-level vision, such as semantic segmentation, by serving as a powerful preprocessing step.

Both quantitative and qualitative evaluation results have validated the effectiveness of ALEN, surpassing recent methods in the state-of-the-art. This method not only enhances image sharpness and fidelity but also opens new avenues

for future research. Moving forward, expanding the large-scale classification dataset used by ALEN and developing specific NIQA metrics to enhance the evaluation of unpaired images are proposed. These enhancements could strengthen the method's robustness across diverse capture conditions and broaden its applicability in practical applications, such as night-time surveillance and imaging in environments with variable and challenging lighting conditions.

Acknowledgements. The author, Ezequiel Perez-Zarate, extends his profound appreciation to Zhejiang Gongshang University and the University of Guadalajara for their substantial support and resources.

References

- [1] Qu, J., Liu, R.W., Gao, Y., Guo, Y., Zhu, F., Wang, F.-Y.: Double domain guided real-time low-light image enhancement for ultra-high-definition transportation surveillance. *IEEE Transactions on Intelligent Transportation Systems* (2024)
- [2] Cao, Y., Liu, M., Liu, S., Wang, X., Lei, L., Zuo, W.: Physics-guided iso-dependent sensor noise modeling for extreme low-light photography. In: *Proceedings of the IEEE/CVF Conference on Computer Vision and Pattern Recognition*, pp. 5744–5753 (2023)
- [3] Li, G., Yang, Y., Qu, X., Cao, D., Li, K.: A deep learning based image enhancement approach for autonomous driving at night. *Knowledge-Based Systems* **213**, 106617 (2021)
- [4] Cui, Z., Qi, G.-J., Gu, L., You, S., Zhang, Z., Harada, T.: Multitask aet with orthogonal tangent regularity for dark object detection. In: *Proceedings of the IEEE/CVF International Conference on Computer Vision*, pp. 2553–2562 (2021)
- [5] Liang, S., Wu, H., Zhen, L., Hua, Q., Garg, S., Kaddoum, G., Hassan, M.M., Yu, K.: Edge yolo: Real-time intelligent object detection system based on edge-cloud cooperation in autonomous vehicles. *IEEE Transactions on Intelligent Transportation Systems* **23**(12), 25345–25360 (2022)
- [6] Ali, M., Yin, B., Bilal, H., Kumar, A., Shaikh, A.M., Rohra, A.: Advanced efficient strategy for detection of dark objects based on spiking network with multi-box detection. *Multimedia Tools and Applications* **83**(12), 36307–36327 (2024)
- [7] Guo, Y., Lu, Y., Guo, Y., Liu, R.W., Chui, K.T.: Intelligent vision-enabled detection of water-surface targets for video surveillance in maritime transportation. *Journal of advanced transportation* **2021**(1), 9470895 (2021)
- [8] Gao, G., Xu, G., Yu, Y., Xie, J., Yang, J., Yue, D.: Mscfnet: A lightweight network with multi-scale context fusion for real-time semantic segmentation. *IEEE Transactions on Intelligent Transportation Systems* **23**(12), 25489–25499 (2021)
- [9] Xia, R., Zhao, C., Zheng, M., Wu, Z., Sun, Q., Tang, Y.: Cmda: Cross-modality domain adaptation for nighttime semantic segmentation. In: *Proceedings of the IEEE/CVF International Conference on Computer Vision*, pp. 21572–21581 (2023)
- [10] Wang, H., Chen, Y., Cai, Y., Chen, L., Li, Y., Sotelo, M.A., Li, Z.: Sfnnet-n: An improved sfnnet algorithm for semantic segmentation of low-light autonomous driving road scenes. *IEEE Transactions on Intelligent Transportation Systems* **23**(11), 21405–21417 (2022)
- [11] Pizer, S.M., Amburn, E.P., Austin, J.D., Cromartie, R., Geselowitz, A., Greer, T., Haar Romeny, B., Zimmerman, J.B., Zuiderveld, K.: Adaptive histogram equalization and its variations. *Computer vision, graphics, and image processing* **39**(3), 355–368 (1987)
- [12] Kaur, M., Kaur, J., Kaur, J.: Survey of contrast enhancement techniques based on histogram equalization. *International Journal of Advanced Computer Science and Applications* **2**(7) (2011)

- [13] Singh, K., Kapoor, R., Sinha, S.K.: Enhancement of low exposure images via recursive histogram equalization algorithms. *Optik* **126**(20), 2619–2625 (2015)
- [14] Wang, Q., Ward, R.K.: Fast image/video contrast enhancement based on weighted thresholded histogram equalization. *IEEE transactions on Consumer Electronics* **53**(2), 757–764 (2007)
- [15] Dale-Jones, R., Tjahjadi, T.: A study and modification of the local histogram equalization algorithm. *Pattern Recognition* **26**(9), 1373–1381 (1993)
- [16] Khan, M.F., Khan, E., Abbasi, Z.A.: Segment dependent dynamic multi-histogram equalization for image contrast enhancement. *Digital Signal Processing* **25**, 198–223 (2014)
- [17] Land, E.H., McCann, J.J.: Lightness and retinex theory. *Josa* **61**(1), 1–11 (1971)
- [18] Choi, D.H., Jang, I.H., Kim, M.H., Kim, N.C.: Color image enhancement using single-scale retinex based on an improved image formation model. In: 2008 16th European Signal Processing Conference, pp. 1–5 (2008). IEEE
- [19] Rahman, Z.-u., Jobson, D.J., Woodell, G.A.: Multi-scale retinex for color image enhancement. In: Proceedings of 3rd IEEE International Conference on Image Processing, vol. 3, pp. 1003–1006 (1996). IEEE
- [20] Jobson, D.J., Rahman, Z.-u., Woodell, G.A.: A multiscale retinex for bridging the gap between color images and the human observation of scenes. *IEEE Transactions on Image processing* **6**(7), 965–976 (1997)
- [21] Rahman, Z.-u., Jobson, D.J., Woodell, G.A.: Retinex processing for automatic image enhancement. *Journal of Electronic imaging* **13**(1), 100–110 (2004)
- [22] Khan, A., Sohail, A., Zahoor, U., Qureshi, A.S.: A survey of the recent architectures of deep convolutional neural networks. *Artificial intelligence review* **53**, 5455–5516 (2020)
- [23] Pan, Z., Yu, W., Yi, X., Khan, A., Yuan, F., Zheng, Y.: Recent progress on generative adversarial networks (gans): A survey. *IEEE access* **7**, 36322–36333 (2019)
- [24] Han, K., Wang, Y., Chen, H., Chen, X., Guo, J., Liu, Z., Tang, Y., Xiao, A., Xu, C., Xu, Y., *et al.*: A survey on vision transformer. *IEEE transactions on pattern analysis and machine intelligence* **45**(1), 87–110 (2022)
- [25] Khan, S., Naseer, M., Hayat, M., Zamir, S.W., Khan, F.S., Shah, M.: Transformers in vision: A survey. *ACM computing surveys (CSUR)* **54**(10s), 1–41 (2022)
- [26] Lee, C., Lee, C., Kim, C.S.: Contrast enhancement based on layered difference representation of 2d histograms. *IEEE Transactions on Image Processing* **22**(12), 5372–5384 (2013)
- [27] Guo, X., Li, Y., Ling, H.: Lime: Low-light image enhancement via illumination map estimation. *IEEE Transactions on image processing* **26**(2), 982–993 (2016)
- [28] Ma, K., Zeng, K., Wang, Z.: Perceptual quality assessment for multi-exposure image fusion. *IEEE Transactions on Image Processing* **24**(11), 3345–3356 (2015)
- [29] Wang, S., Zheng, J., Hu, H.M., *et al.*: Naturalness preserved enhancement algorithm for non-uniform illumination images. *IEEE Transactions on Image Processing* **22**(9), 3538–3548 (2013)
- [30] Perez-Zarate, E., Ramos-Soto, O., Rodríguez-Esparza, E., Aguilar, G.: Loli-ia: low-light image enhancement algorithm. In: Applications of Machine Learning 2023, vol. 12675, pp. 230–245 (2023). SPIE
- [31] Ibrahim, H., Kong, N.S.P.: Brightness preserving dynamic histogram equalization for image contrast enhancement. *IEEE Transactions on Consumer Electronics* **53**(4), 1752–1758 (2007)
- [32] Abdullah-Al-Wadud, M., Kabir, M.H., Dewan, M.A.A., Chae, O.: A dynamic

- histogram equalization for image contrast enhancement. *IEEE transactions on consumer electronics* **53**(2), 593–600 (2007)
- [33] Hitam, M.S., Awalludin, E.A., Yussof, W.N.J.H.W., Bachok, Z.: Mixture contrast limited adaptive histogram equalization for underwater image enhancement. In: 2013 International Conference on Computer Applications Technology (ICCAT), pp. 1–5 (2013). IEEE
- [34] Thepade, S.D., Pardhi, P.M.: Contrast enhancement with brightness preservation of low light images using a blending of clahe and bpdhe histogram equalization methods. *International Journal of Information Technology* **14**(6), 3047–3056 (2022)
- [35] Han, Y., Chen, X., Zhong, Y., Huang, Y., Li, Z., Han, P., Li, Q., Yuan, Z.: Low-illumination road image enhancement by fusing retinex theory and histogram equalization. *Electronics* **12**(4), 990 (2023)
- [36] Land, E.H., McCann, J.J.: Lightness and retinex theory. *Josa* **61**(1), 1–11 (1971)
- [37] Reflectance–Illuminance, B.: Retinex image processing: improving the visual realism of color images. *Int. J. Inf. Technol* **4**(2), 371–377 (2011)
- [38] Hussein, R.R., Hamodi, Y.I., Roaa, A.S.: Retinex theory for color image enhancement: A systematic review. *International Journal of Electrical and Computer Engineering* **9**(6), 5560 (2019)
- [39] Wei, C., Wang, W., Yang, W., Liu, J.: Deep retinex decomposition for low-light enhancement. *arXiv preprint arXiv:1808.04560* (2018)
- [40] Wu, W., Weng, J., Zhang, P., Wang, X., Yang, W., Jiang, J.: Uretinex-net: Retinex-based deep unfolding network for low-light image enhancement. In: Proceedings of the IEEE/CVF Conference on Computer Vision and Pattern Recognition, pp. 5901–5910 (2022)
- [41] Yi, X., Xu, H., Zhang, H., Tang, L., Ma, J.: Diff-retinex: Rethinking low-light image enhancement with a generative diffusion model. In: Proceedings of the IEEE/CVF International Conference on Computer Vision, pp. 12302–12311 (2023)
- [42] Cai, Y., Bian, H., Lin, J., Wang, H., Timofte, R., Zhang, Y.: Retinexformer: One-stage retinex-based transformer for low-light image enhancement. In: Proceedings of the IEEE/CVF International Conference on Computer Vision, pp. 12504–12513 (2023)
- [43] Bai, J., Yin, Y., He, Q.: Retinexmamba: Retinex-based mamba for low-light image enhancement. *arXiv preprint arXiv:2405.03349* (2024)
- [44] Zhang, Q., Nie, Y., Zheng, W.-S.: Dual illumination estimation for robust exposure correction. In: *Computer Graphics Forum*, vol. 38, pp. 243–252 (2019). Wiley Online Library
- [45] Zhang, F., Shao, Y., Sun, Y., Zhu, K., Gao, C., Sang, N.: Unsupervised low-light image enhancement via histogram equalization prior. *arXiv preprint arXiv:2112.01766* (2021)
- [46] Jin, Y., Yang, W., Tan, R.T.: Unsupervised night image enhancement: When layer decomposition meets light-effects suppression. In: *European Conference on Computer Vision*, pp. 404–421 (2022). Springer
- [47] Ma, L., Ma, T., Liu, R., Fan, X., Luo, Z.: Toward fast, flexible, and robust low-light image enhancement. In: Proceedings of the IEEE/CVF Conference on Computer Vision and Pattern Recognition, pp. 5637–5646 (2022)
- [48] Liang, Z., Li, C., Zhou, S., Feng, R., Loy, C.C.: Iterative prompt learning for unsupervised backlit image enhancement. In: Proceedings of the IEEE/CVF International Conference on Computer Vision, pp. 8094–8103 (2023)
- [49] Chen, X., Yu, Y.: An unsupervised low-light image enhancement method for improving

- v-slam localization in uneven low-light construction sites. *Automation in Construction* **162**, 105404 (2024)
- [50] Xu, H., Liu, X., Zhang, H., Wu, X., Zuo, W.: Degraded structure and hue guided auxiliary learning for low-light image enhancement. *Knowledge-Based Systems* **295**, 111779 (2024)
- [51] Wang, L.-W., Liu, Z.-S., Siu, W.-C., Lun, D.P.: Lightening network for low-light image enhancement. *IEEE Transactions on Image Processing* **29**, 7984–7996 (2020)
- [52] Guo, C., Li, C., Guo, J., Loy, C.C., Hou, J., Kwong, S., Cong, R.: Zero-reference deep curve estimation for low-light image enhancement. In: *Proceedings of the IEEE/CVF Conference on Computer Vision and Pattern Recognition*, pp. 1780–1789 (2020)
- [53] Liu, R., Ma, L., Zhang, J., Fan, X., Luo, Z.: Retinex-inspired unrolling with cooperative prior architecture search for low-light image enhancement. In: *Proceedings of the IEEE/CVF Conference on Computer Vision and Pattern Recognition*, pp. 10561–10570 (2021)
- [54] Zheng, C., Shi, D., Shi, W.: Adaptive unfolding total variation network for low-light image enhancement. In: *Proceedings of the IEEE/CVF International Conference on Computer Vision*, pp. 4439–4448 (2021)
- [55] Fan, C.-M., Liu, T.-J., Liu, K.-H.: Half wavelet attention on m-net+ for low-light image enhancement. In: *2022 IEEE International Conference on Image Processing (ICIP)*, pp. 3878–3882 (2022). IEEE
- [56] Wang, Y., Wan, R., Yang, W., Li, H., Chau, L.-P., Kot, A.: Low-light image enhancement with normalizing flow. In: *Proceedings of the AAAI Conference on Artificial Intelligence*, vol. 36, pp. 2604–2612 (2022)
- [57] Cui, Z., Li, K., Gu, L., Su, S., Gao, P., Jiang, Z., Qiao, Y., Harada, T.: You only need 90k parameters to adapt light: a light weight transformer for image enhancement and exposure correction. *arXiv preprint arXiv:2205.14871* (2022)
- [58] Ma, L., Jin, D., An, N., Liu, J., Fan, X., Luo, Z., Liu, R.: Bilevel fast scene adaptation for low-light image enhancement. *International Journal of Computer Vision*, 1–19 (2023)
- [59] Guo, X., Hu, Q.: Low-light image enhancement via breaking down the darkness. *International Journal of Computer Vision* **131**(1), 48–66 (2023)
- [60] Fu, Z., Yang, Y., Tu, X., Huang, Y., Ding, X., Ma, K.-K.: Learning a simple low-light image enhancer from paired low-light instances. In: *Proceedings of the IEEE/CVF Conference on Computer Vision and Pattern Recognition*, pp. 22252–22261 (2023)
- [61] Hasinoff, S.W., Sharlet, D., Geiss, R., Adams, A., Barron, J.T., Kainz, F., Chen, J., Levoy, M.: Burst photography for high dynamic range and low-light imaging on mobile cameras. *ACM Transactions on Graphics (ToG)* **35**(6), 1–12 (2016)
- [62] Lv, F., Li, Y., Lu, F.: Attention guided low-light image enhancement with a large scale low-light simulation dataset. *International Journal of Computer Vision* **129**(7), 2175–2193 (2021)
- [63] Bychkovsky, V., Paris, S., Chan, E., Durand, F.: Learning photographic global tonal adjustment with a database of input/output image pairs. In: *CVPR 2011*, pp. 97–104 (2011). IEEE
- [64] Zeng, H., Cai, J., Li, L., *et al.*: Learning image-adaptive 3d lookup tables for high performance photo enhancement in real-time. *IEEE Transactions on Pattern Analysis and Machine Intelligence* **14**(8), 2058–2073 (2020)
- [65] Lin, T.-Y., Maire, M., Belongie, S., Hays, J., Perona, P., Ramanan, D., Dollár, P., Zitnick, C.L.: Microsoft coco: Common objects in context. In: *Computer Vision–ECCV 2014: 13th European Conference, Zurich, Switzerland,*

- September 6-12, 2014, Proceedings, Part V 13, pp. 740–755 (2014). Springer
- [66] Deng, J., Dong, W., Socher, R., Li, L.-J., Li, K., Fei-Fei, L.: Imagenet: A large-scale hierarchical image database. In: 2009 IEEE Conference on Computer Vision and Pattern Recognition, pp. 248–255 (2009). Ieee
- [67] PyTorch: BCELoss. <https://pytorch.org/docs/stable/generated/torch.nn.BCELoss.html>. Accessed: June 1, 2023 (2019)
- [68] PyTorch: MSELoss. <https://pytorch.org/docs/stable/generated/torch.nn.MSELoss.html>. Accessed: June 1, 2023 (2019)
- [69] Wang, Z., Bovik, A.C., Sheikh, H.R., Simoncelli, E.P.: Image quality assessment: from error visibility to structural similarity. *IEEE transactions on image processing* **13**(4), 600–612 (2004)
- [70] Johnson, J., Alahi, A., Fei-Fei, L.: Perceptual losses for real-time style transfer and super-resolution. In: Computer Vision–ECCV 2016: 14th European Conference, Amsterdam, The Netherlands, October 11-14, 2016, Proceedings, Part II 14, pp. 694–711 (2016). Springer
- [71] Simonyan, K., Zisserman, A.: Very deep convolutional networks for large-scale image recognition. *arXiv preprint arXiv:1409.1556* (2014)
- [72] Paszke, A., Gross, S., Massa, F., Lerer, A., Bradbury, J., Chanan, G., Killeen, T., Lin, Z., Gimelshein, N., Antiga, L., et al.: Pytorch: An imperative style, high-performance deep learning library. *Advances in neural information processing systems* **32** (2019)
- [73] Kingma, D.P., Ba, J.: Adam: A method for stochastic optimization. *arXiv preprint arXiv:1412.6980* (2014)
- [74] Guo, X., Hu, Q.: Low-light image enhancement via breaking down the darkness. *International Journal of Computer Vision* **131**(1), 48–66 (2023)
- [75] Hou, J., Zhu, Z., Hou, J., Liu, H., Zeng, H., Yuan, H.: Global structure-aware diffusion process for low-light image enhancement. *Advances in Neural Information Processing Systems* **36** (2024)
- [76] Wang, Z., Bovik, A.C.: A universal image quality index. *IEEE signal processing letters* **9**(3), 81–84 (2002)
- [77] Zhang, R., Isola, P., Efros, A.A., Shechtman, E., Wang, O.: The unreasonable effectiveness of deep features as a perceptual metric. In: Proceedings of the IEEE Conference on Computer Vision and Pattern Recognition, pp. 586–595 (2018)
- [78] Mittal, A., Soundararajan, R., Bovik, A.C.: Making a “completely blind” image quality analyzer. *IEEE Signal processing letters* **20**(3), 209–212 (2012)
- [79] Wang, T., Zhang, K., Shen, T., Luo, W., Stenger, B., Lu, T.: Ultra-high-definition low-light image enhancement: A benchmark and transformer-based method. In: Proceedings of the AAAI Conference on Artificial Intelligence, vol. 37, pp. 2654–2662 (2023)
- [80] Hai, J., Xuan, Z., Yang, R., Hao, Y., Zou, F., Lin, F., Han, S.: R2rnet: Low-light image enhancement via real-low to real-normal network. *Journal of Visual Communication and Image Representation* **90**, 103712 (2023)
- [81] Morawski, I., Chen, Y.A., Lin, Y.S., et al.: Nod: Taking a closer look at detection under extreme low-light conditions with night object detection dataset. *arXiv preprint arXiv:2110.10364* (2021)
- [82] Kirillov, A., Mintun, E., Ravi, N., Mao, H., Rolland, C., Gustafson, L., Xiao, T., Whitehead, S., Berg, A.C., Lo, W.-Y., et al.: Segment anything. In: Proceedings of the IEEE/CVF International Conference on Computer Vision, pp. 4015–4026 (2023)